# Supplemental Information: Optical polarization evolution and transmission in multi-Ranvier-node myelin sheath waveguides

**Emily Frede**[1], **Hadi Zadeh-Haghighi**[1,2,3], **and Christoph Simon**[1,2,3]

[1]Department of Physics and Astronomy, University of Calgary, Calgary, AB T2N 1N4, Canada
[2]Institute for Quantum Science and Technology, University of Calgary, Calgary, AB T2N 1N4, Canada
[3]Hotchkiss Brain Institute, University of Calgary, Calgary, AB T2N 1N4, Canada
[*]corresponding.author@email.example
[+]these authors contributed equally to this work

## ABSTRACT

In neuroscience it is compelling to consider all possible information transfer between neurons, in order to fully understand processing in the brain. It has been suggested that photonic communication may be possible along axonal connections, especially through the myelin sheath as a waveguide due to its high refractive index. There is already a good deal of theoretical and experimental evidence for light guidance in the myelin sheath despite realistic optical imperfections, however the feature of light polarization remains largely unexplored. Polarization evolution is relevant to our interest in considering neural communication via the exchange of biophotons, which have been observed in the brain predominantly within the visible spectral range. It is presently unclear whether polarization-encoded information could be preserved within the myelin sheath. We simulate propagation of a single-wavelength mode through a myelinated axon structure with multiple Ranvier nodes. This allows us to observe polarization change and test the assumption of exponentiated transmission loss through multiple Ranvier nodes for guided light along myelin sheath waveguides. These results provide important context for information transmission facilitated by biophotons, leaving open the possibilities of both classical and quantum photonic communication within the brain.

## Software and the FDTD Method

This project utilised ANSYS Lumerical FDTD software[1] (version: 8.26.2779) to construct models and run simulations. This software uses the Finite Difference Time Domain (FDTD) method[2] to solve Maxwell's equations as written in Equation 1 for models on the nanometer scale, which allows us to calculate modes and simulate light propagation in myelinated axon models. $\vec{H}$, $\vec{E}$, $\vec{D}$ denote the magnetic, electric, and displacement fields respectively; $\varepsilon_r(\omega) = n^2$ is the complex relative dielectric constant which depends upon the refractive index $n$ of the material.

$$\begin{aligned} \frac{\partial \vec{D}}{\partial t} &= \nabla \times \vec{H} \\ \vec{D}(\omega) &= \varepsilon_0 \varepsilon_r(\omega) \vec{E}(\omega) \\ \frac{\partial \vec{H}}{\partial t} &= -\frac{1}{\mu_0} \nabla \times \vec{E} \end{aligned} \tag{1}$$

Maxwell's equations (Equation 1) are split into two sets of equations (transverse electric and transverse magnetic) which can be solved with the FDTD method. The FDTD method solves for the $\vec{E}$ and $\vec{H}$ field components on a discrete spatial and temporal grid and governed by the Yee cell paradigm. The spatial grid used to solve for these field components is also referred to as the simulation mesh.

Default settings of the software were used for our simulations. We use the default auto non-uniform simulation mesh, which varies size of mesh cells according to minimization of numerical dispersion and improvement of interface resolution. This allows for optimization of accuracy and efficiency of the simulations. Simulation time is adjusted to 3700 fs for simulations of light propagation across 500 $\mu$m, to ensure sufficient time for the light to propagate through the entire simulation region. (This was based off the ratio between good light propagation distance and simulation time for a simulation with insufficient simulation time.)

## Myelin sheath modes, extended

Here we present the modes six through twelve as calculated by the software, named according to established convention[3–5]. (The first six are presented in Appendix A.) Note that since $\mathrm{HE}^{e}_{31}$ and $\mathrm{HE}^{o}_{31}$ are degenerate, with virtually the same refractive index, they are interchangeable in their order. We have unintentionally recorded $\mathrm{HE}^{o}_{31}$ twice.

As discussed in Appendix A, we have also recorded the effective index $n_{eff}$ for each of the modes. $\mathrm{HE}^{o}_{31}$ shown in Fig. 1a – 1b (and its duplicate in Fig. 1c – 1d), has the six-point star polarization pattern and an effective index $n_{eff} = 1.4000$. $\mathrm{EH}^{e}_{11}$ in Fig. 1e – 1f and $\mathrm{EH}^{o}_{11}$ in Fig. 1g – 1h have dipole polarization patterns and an effective index of $n_{eff} = 1.3998$. $\mathrm{EH}^{e}_{21}$ in Fig. 1i – 1j and $\mathrm{EH}^{o}_{21}$ in Fig. 1k – 1l have double-dipole polarization patterns and have an effective index of $n_{eff} = 1.3874$.

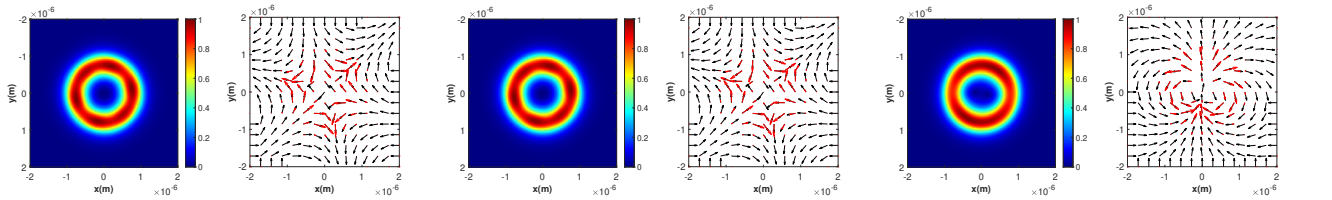

**(a)** Electric field magnitude plot for $\mathrm{HE}^{o}_{31}$.

**(b)** Electric field vector plot for $\mathrm{HE}^{o}_{31}$.

**(c)** Electric field magnitude plot for $\mathrm{HE}^{o}_{31}$, duplicate.

**(d)** Electric field vector plot for $\mathrm{HE}^{o}_{31}$, duplicate.

**(e)** Electric field magnitude plot for $\mathrm{EH}^{e}_{11}$.

**(f)** Electric field vector plot for $\mathrm{EH}^{e}_{11}$.

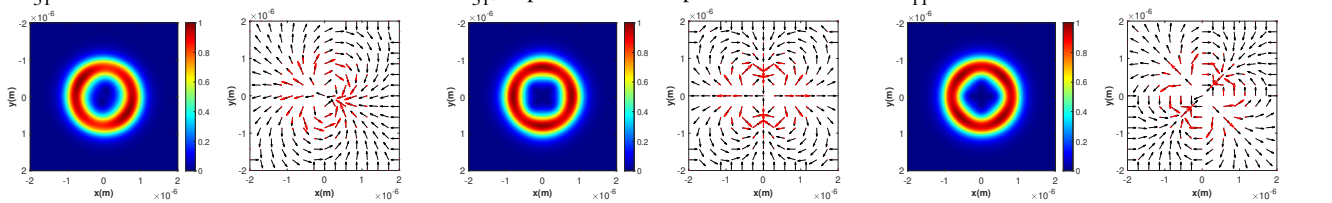

**(g)** Electric field magnitude plot for $\mathrm{EH}^{o}_{11}$.

**(h)** Electric field vector plot for $\mathrm{EH}^{o}_{11}$.

**(i)** Electric field magnitude plot for $\mathrm{EH}^{e}_{21}$.

**(j)** Electric field vector plot for $\mathrm{EH}^{e}_{21}$.

**(k)** Electric field magnitude plot for $\mathrm{EH}^{o}_{21}$.

**(l)** Electric field vector plot for $\mathrm{EH}^{o}_{21}$.

**Figure 1.** Modes six through twelve calculated by the software (as ordered by decreasing effective index), named according to established convention[3–5]. Modes are calculated over the cross-section of the model at the source ($z = 0\,\mu$m). Input light amplitude is $1\,\mathrm{V/m}$. Plots (a), (c), (e), (g), (i), (k) depict electric field magnitude. Electric field magnitudes given in units of $\mathrm{V/m}$. Plots (b), (d), (f), (h), (j), (l) depict electric field vectors; black lines depict the normalized three-dimensional electric field vector at a given position, red arrows depict the magnitude-scaled three-dimensional electric field vector at a given position. The $E_z$ component is negligible in all cases, on the order of $10^{-6}\,\mathrm{V/m}$ or less.

## Electric field profiles, extended

Here we present further electric field profiles at cross-sections every $25\,\mu$m through the myelinated axon model, as a mode propagates through the myelin sheath. These results are presented in Fig. 2, 3, 4, 5, 6. Recall the source is located at $z = 0\,\mu$m, there are $2\,\mu$m Ranvier nodes located at $z = 100, 200, 300, 400\,\mu$m, and the simulation region spans $500\,\mu$m along the model from the location of the source.

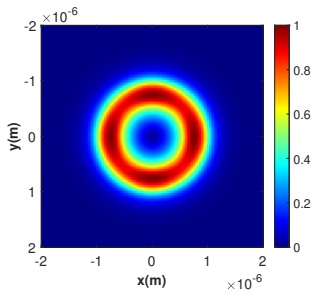


**(a)** Electric field magnitude plot of input $\mathrm{HE}_{21}^{o}$ mode.

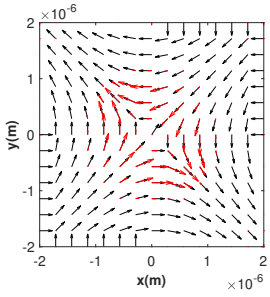


**(b)** Electric field vector plot of input $\mathrm{HE}_{21}^{o}$ mode.

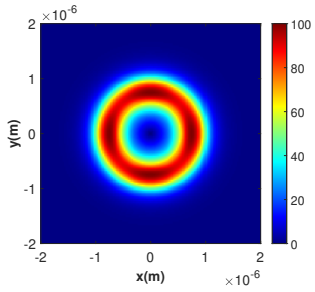


**(c)** Electric field magnitude plot at $25\,\mu$m.

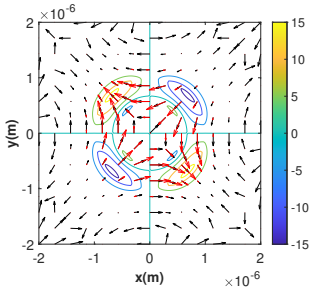


**(d)** Electric field vector plot at $25\,\mu$m.

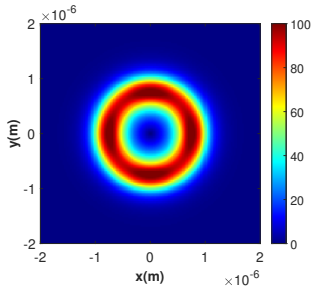


**(e)** Electric field magnitude plot at $50\,\mu$m.

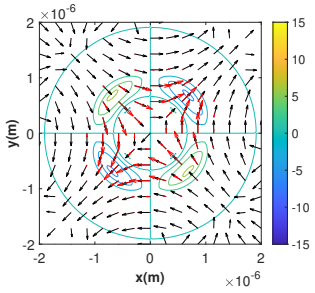


**(f)** Electric field vector plot at $50\,\mu$m.

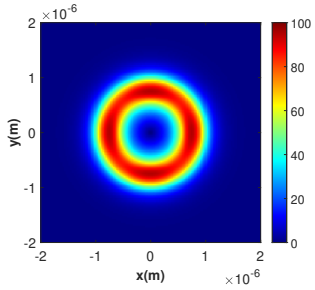


**(g)** Electric field magnitude plot at $75\,\mu$m.

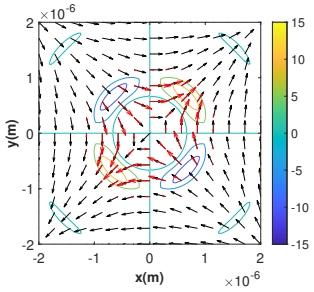


**(h)** Electric field vector plot at $75\,\mu$m.

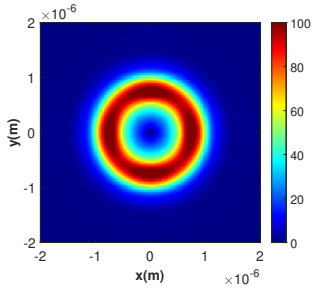


**(i)** Electric field magnitude plot at $100\,\mu$m.

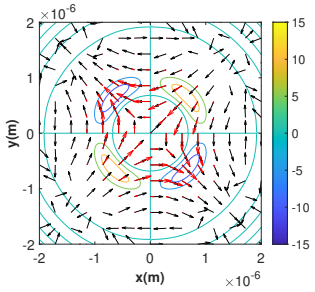


**(j)** Electric field vector plot at $100\,\mu$m.

**Figure 2.** Electric field profiles of calculated input mode $\mathrm{HE}_{21}^{o}$ and cross-sections of the four-Ranvier-node myelinated axon structure at positions $25, 50, 75, 100\,\mu$m. The mode source is located at $0\,\mu$m, input amplitude is $100\,\mathrm{V/m}$. Ranvier nodes are $2\,\mu$m long and begin at $z = 100, 200, 300, 400\,\mu$m. Plots (a), (c), (e), (g), (i), (k) depict electric field magnitude. Plots (b), (d), (f), (h), (j), (l) depict electric field vectors; black lines depict the normalized three-dimensional electric field vector at a given position, red arrows depict the magnitude-scaled three-dimensional electric field vector at a given position; color-coded contour lines depict magnitude of $E_z$. Electric field magnitudes given in units of $\mathrm{V/m}$.

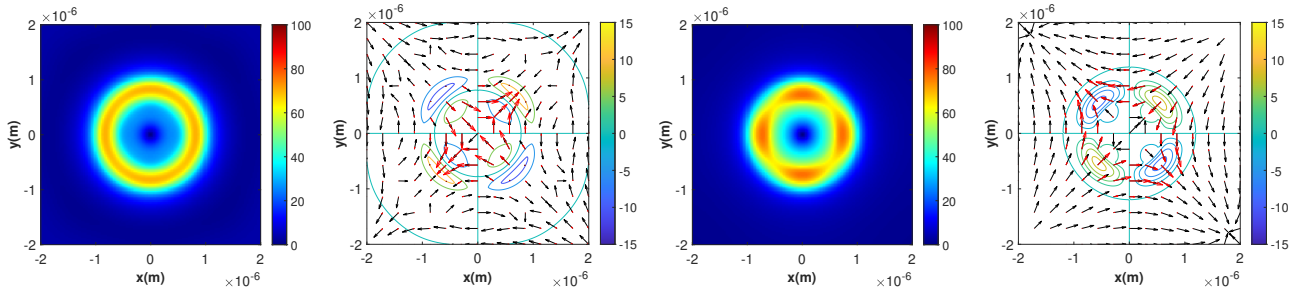


**(a)** Electric field magnitude plot at 125 $\mu$m. **(b)** Electric field vector plot at 125 $\mu$m. **(c)** Electric field magnitude plot at 150 $\mu$m. **(d)** Electric field vector plot at 150 $\mu$m.

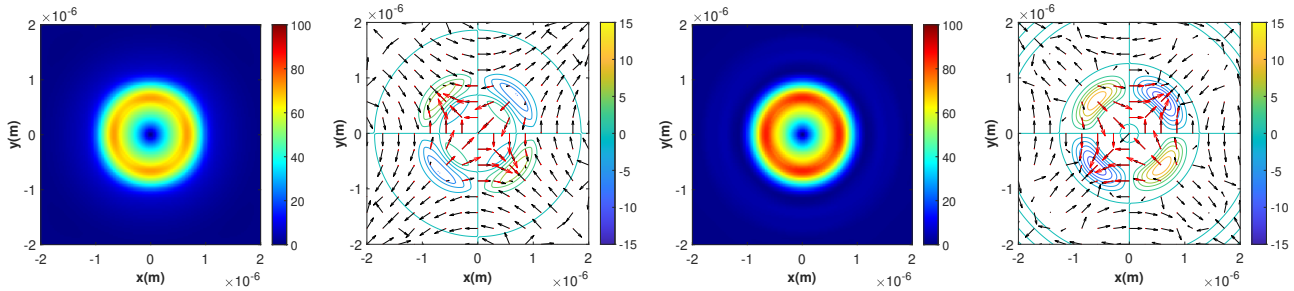


**(e)** Electric field magnitude plot at 175 $\mu$m. **(f)** Electric field vector plot at 175 $\mu$m. **(g)** Electric field magnitude plot at 200 $\mu$m. **(h)** Electric field vector plot at 200 $\mu$m.

**Figure 3.** Electric field profiles of cross-sections of the four-Ranvier-node myelinated axon structure at positions $125, 150, 175, 200\,\mu$m. The mode source is located at $0\,\mu$m, input amplitude is $100\,\mathrm{V/m}$. Ranvier nodes are $2\,\mu$m long and begin at $z = 100, 200, 300, 400\,\mu$m. Plots (a), (c), (e), (g), (i), (k) depict electric field magnitude. Plots (b), (d), (f), (h), (j), (l) depict electric field vectors; black lines depict the normalized three-dimensional electric field vector at a given position, red arrows depict the magnitude-scaled three-dimensional electric field vector at a given position; color-coded contour lines depict magnitude of $E_z$. Electric field magnitudes given in units of $\mathrm{V/m}$.

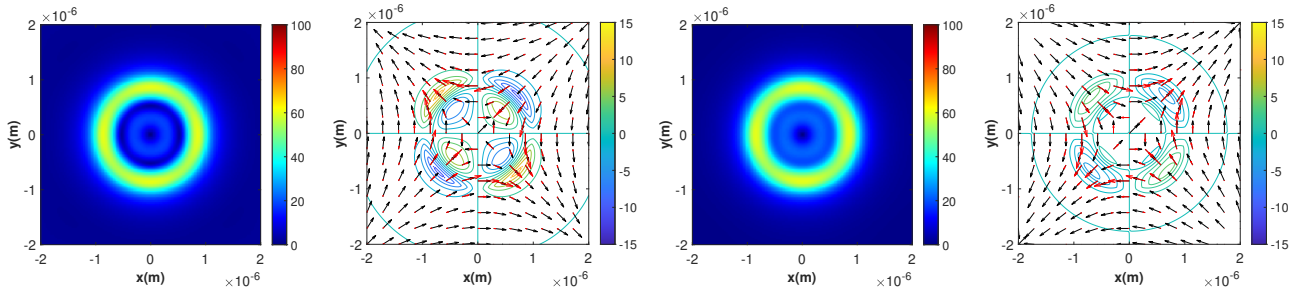


**(a)** Electric field magnitude plot at 225 $\mu$m. **(b)** Electric field vector plot at 225 $\mu$m. **(c)** Electric field magnitude plot at 250 $\mu$m. **(d)** Electric field vector plot at 250 $\mu$m.

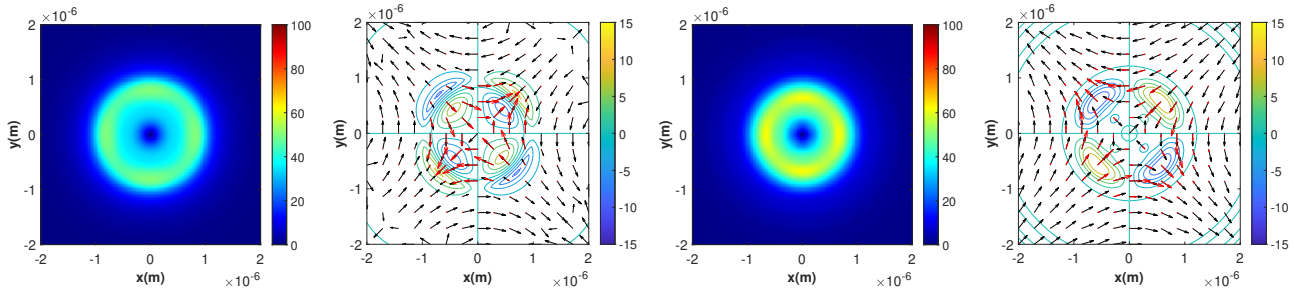


**(e)** Electric field magnitude plot at 275 $\mu$m. **(f)** Electric field vector plot at 275 $\mu$m. **(g)** Electric field magnitude plot at 300 $\mu$m. **(h)** Electric field vector plot at 300 $\mu$m.

**Figure 4.** Electric field profiles of cross-sections of the four-Ranvier-node myelinated axon structure at positions $225, 250, 275, 300\,\mu$m. The mode source is located at $0\,\mu$m, input amplitude is $100\,\mathrm{V/m}$. Ranvier nodes are $2\,\mu$m long and begin at $z = 100, 200, 300, 400\,\mu$m. Plots (a), (c), (e), (g), (i), (k) depict electric field magnitude. Plots (b), (d), (f), (h), (j), (l) depict electric field vectors; black lines depict the normalized three-dimensional electric field vector at a given position, red arrows depict the magnitude-scaled three-dimensional electric field vector at a given position; color-coded contour lines depict magnitude of $E_z$. Electric field magnitudes given in units of $\mathrm{V/m}$.

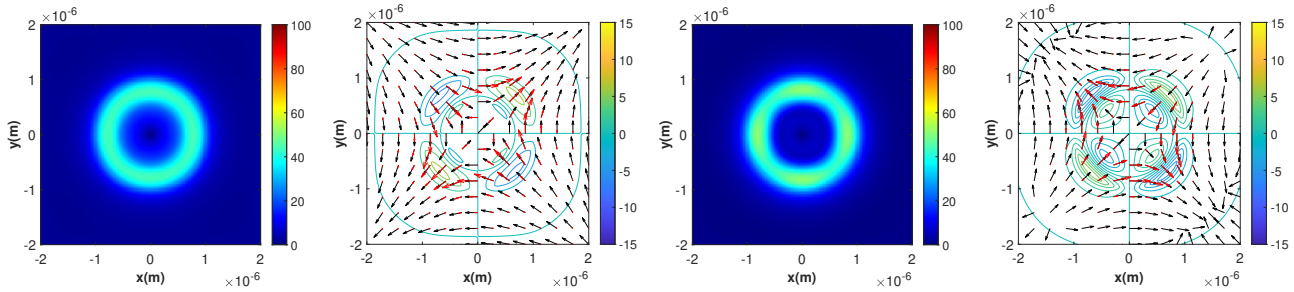


**(a)** Electric field magnitude plot at 325 $\mu$m. **(b)** Electric field vector plot at 325 $\mu$m. **(c)** Electric field magnitude plot at 350 $\mu$m. **(d)** Electric field vector plot at 350 $\mu$m.

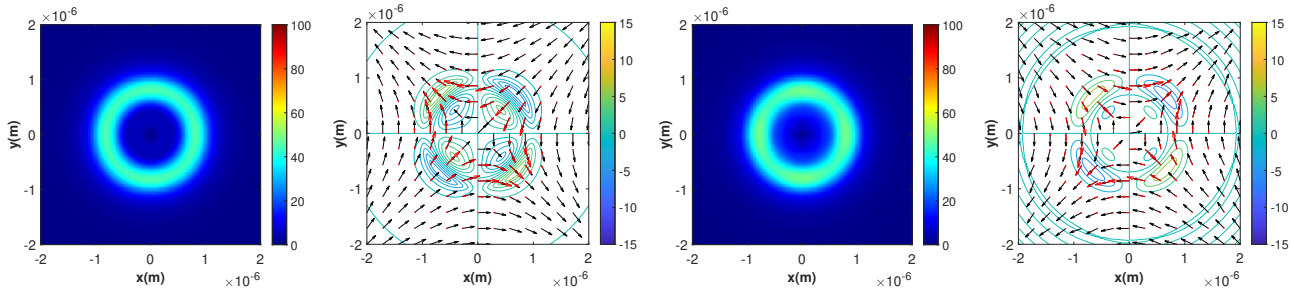


**(e)** Electric field magnitude plot at 375 $\mu$m. **(f)** Electric field vector plot at 375 $\mu$m. **(g)** Electric field magnitude plot at 400 $\mu$m. **(h)** Electric field vector plot at 400 $\mu$m.

**Figure 5.** Electric field profiles of cross-sections of the four-Ranvier-node myelinated axon structure at positions $325, 350, 375, 400\,\mu$m. The mode source is located at $0\,\mu$m, input amplitude is $100\,\mathrm{V/m}$. Ranvier nodes are $2\,\mu$m long and begin at $z = 100, 200, 300, 400\,\mu$m. Plots (a), (c), (e), (g), (i), (k) depict electric field magnitude. Plots (b), (d), (f), (h), (j), (l) depict electric field vectors; black lines depict the normalized three-dimensional electric field vector at a given position, red arrows depict the magnitude-scaled three-dimensional electric field vector at a given position; color-coded contour lines depict magnitude of $E_z$. Electric field magnitudes given in units of $\mathrm{V/m}$.

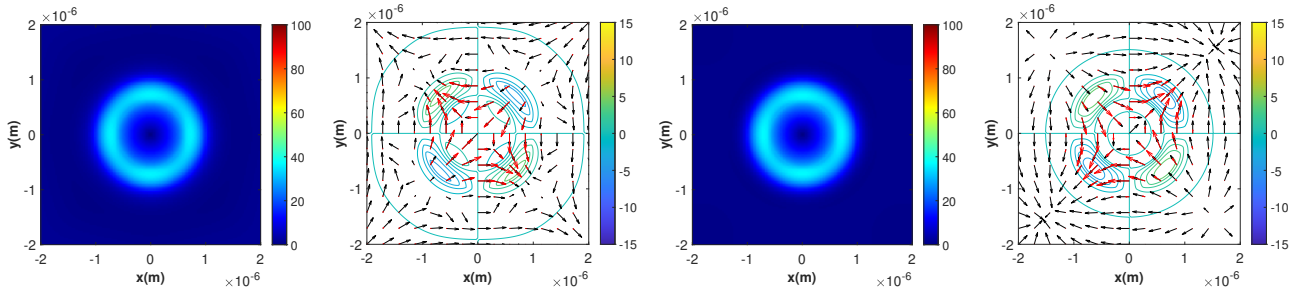


**(a)** Electric field magnitude plot at 425 $\mu$m. **(b)** Electric field vector plot at 425 $\mu$m. **(c)** Electric field magnitude plot at 450 $\mu$m. **(d)** Electric field vector plot at 450 $\mu$m.

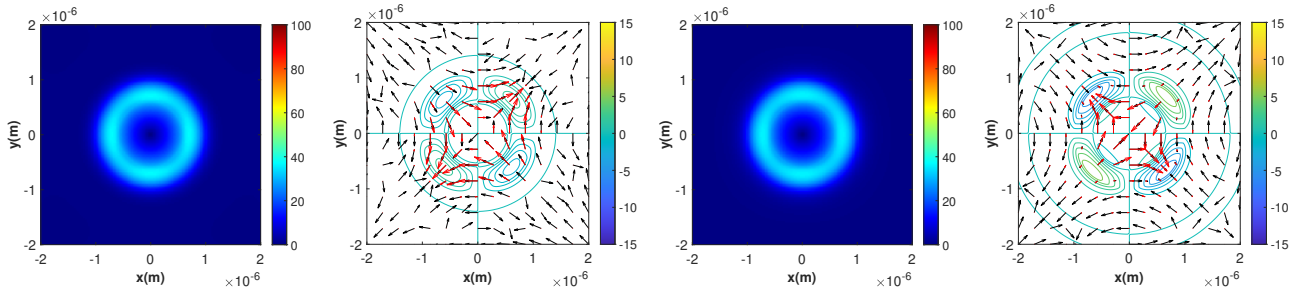


**(e)** Electric field magnitude plot at 475 $\mu$m. **(f)** Electric field vector plot at 475 $\mu$m. **(g)** Electric field magnitude plot at 500 $\mu$m. **(h)** Electric field vector plot at 500 $\mu$m.

**Figure 6.** Electric field profiles of cross-sections of the four-Ranvier-node myelinated axon structure at positions $425, 450, 475, 500\,\mu$m. The mode source is located at $0\,\mu$m, input amplitude is $100\,\mathrm{V/m}$. Ranvier nodes are $2\,\mu$m long and begin at $z = 100, 200, 300, 400\,\mu$m. Plots (a), (c), (e), (g), (i), (k) depict electric field magnitude. Plots (b), (d), (f), (h), (j), (l) depict electric field vectors; black lines depict the normalized three-dimensional electric field vector at a given position, red arrows depict the magnitude-scaled three-dimensional electric field vector at a given position; color-coded contour lines depict magnitude of $E_z$. Electric field magnitudes given in units of $\mathrm{V/m}$.

## References


1. Ansys lumerical inc. (version: 8.26.2779) (2022).
2. Kim, S.-S. Finite difference time domain (fdtd) solver introduction (2022).
3. Zeng, H., Zhang, Y., Ma, Y. & Li, S. Electromagnetic modeling and simulation of the biophoton propagation in myelinated axon waveguide. *Appl. optics (2004)* **61**, 4013– (2022).
4. Black, R. J. *Optical waveguide modes polarization, coupling, and symmetry* (McGraw-Hill, New York, 2010).
5. Yirmiyahu, Y., Niv, A., Biener, G., Kleiner, V. & Hasman, E. Excitation of a single hollow waveguide mode using inhomogeneous anisotropic subwavelength structures. *Opt. express* **15**, 13404–13414 (2007).